Inorganic Chemistry

pubs.acs.org/IC Article

V═O Functionalized $\{Tm_2\}$−Organic Framework Designed by Postsynthesis Modification for Catalytic Chemical Fixation of CO_2 and Oxidation of Mustard Gas

Hongtai Chen, Liming Fan, Tuoping Hu, and Xiutang Zhang*

Cite This: *Inorg. Chem.* 2021, 60, 5005−5013 Read Online

ACCESS | Metrics & More | Article Recommendations | Supporting Information

ABSTRACT: In terms of recently documented references, the introduction of V═O units into porous MOF/COF frameworks can greatly improve their original performance and expand their application prospects due to a change in their electronegativity. In this work, by a cation-exchange strategy, a consummate combination of separate 4f $[Tm_2(CO_2)_8]$ SBUs and 3d $[V^{IV}O(H_2O)_2]$ units generated the functionalized porous metal−organic framework $\{(Me_2NH_2)_2[VO(H_2O)][Tm_2(BDCP)_2]\cdot 3DMF\cdot 3H_2O\}_n$ (**NUC-11**), in which $[Tm_2(CO_2)_8]$ SBUs constitute the fundamental 3D host framework of $\{[Tm_2](BDCP)_2\}_n$ along with $[V^{IV}O(H_2O)_2]$ units being further docked on the inner wall of channels by covalent bonds. Significantly, **NUC-11** represents the first example of V═O modified porous MOFs, in which uncoordinated carboxylic groups ($-CO_2H$) further grasp the functional $[V^{IV}O(H_2O)_2]$ units on the initial basic skeleton along with the formation of covalent bonds as fixed ropes. Furthermore, activated samples of **NUC-11** displayed a good catalytic performance for the chemical synthesis of carbonates from related epoxides and CO_2 with high conversion rate. Moreover, by employing **NUC-11** as a catalyst, a simulator of mustard gas, 2-chloroethyl ethyl sulfide, could be quickly and efficiently oxidized into low-toxicity products of oxidized sulfoxide (CEESO). Thus, this study offers a brand new view for the design and synthesis of functional-units-modified porous MOFs, which could be potentially applied as an excellent candidate in the growing field of efficient catalysis.

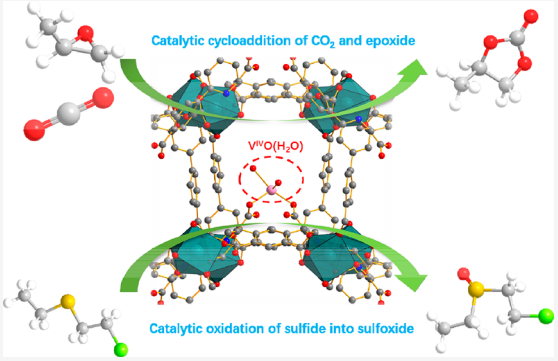

■ INTRODUCTION

Over the past decade, much attention has been paid to the self-assembly of porous metal−organic frameworks (MOFs), which have the characteristics of large specific surface area and can be potentially applied as gas separators and collectors, catalysts for chemical reactions, molecular sensors, etc.[1−8] Usually, the substitution of metal cations or organic ligands leads to a completely novel topology along with realization of the goal of functionalization, on which basis huge numbers of MOFs with unique specific functions have been documented.[9−14] Moreover, in recent years, in order to enhance the functional characteristics, in-depth research has concentrated on increasing the specific surface area and adjustable aperture of targeted MOFs by the typical strategies of employing functional ligands or mixed ligands, introducing templates postmodification with polar functional groups. Thus, a great number of MOFs combining multistage pore structures and specific functions have emerged. However, in comparison to d-block metal based MOFs, the adsorption and catalytic performance exhibited by porous Ln-MOFs have rarely been reported,[15−19] which could be attributed to the defects of hard-sphere and coordination-geometry flexibility from Ln^{3+} ions habitually leading to a low-dimensional framework or interwoven structure. Although it is a huge challenge to successfully assemble the targeted porous Ln-MOFs, their excellent properties in the aspects of selective separation and storage, luminescence and recognition, and catalysis continue to attract remarkable attention from many scientists. Especially, the fact that the rich coordination geometry of Ln^{3+} ions due to the ratio of charge to radius (Z/R) and abundant hybrid orbitals of $f^n d^{2+m} sp^3$ ($n = 0-3$, $m = 1-3$) gives them a wide coordination number range, which grants octa- or nonacoordinated Ln^{3+} ions the ability to polarize small guest molecules, such as CO_2, SO_2, and H_2S.[20,21] Recently, one porous Eu-MOF reported by Zhao and co-workers exhibited an efficient catalytic performance for the chemical fixation of CO_2,[22] which confirmed that Ln-MOFs are subjects worthy of study due to the fact that the high coordination characteristics of Ln^{III} ions give them ideal Lewis acid sites. Therefore, the exploration of syntheses and

Received: January 7, 2021
Published: March 15, 2021

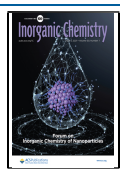

https://dx.doi.org/10.1021/acs.inorgchem.1c00053
Inorg. Chem. 2021, 60, 5005−5013

optimization for Ln-based host skeletons by increasing highly active sites to achieve targeted catalysts has become inevitable.

In addition, to exploit types of new catalytic materials that have excellent characteristics including safety, high efficiency, convenient recyclability, and reusability is momentous from the perspective of applications. Under this premise, several representative categories of multihole functional materials including COFs (covalent-organic frameworks), POPs (porous-organic polymers), and MOFs have aroused the enthusiasm of researchers,[23−33] which has led to the design and syntheses of novel catalytic models. Recently, on the basis of the principle of coordination binding, vanadium oxide units were successfully docked on the skeleton of COFs by Ma and co-workers to form the heterogeneous catalysts VO-PyTTA-2,3-DHTA and VOTAPT-2,3-DHTA, which displayed excellent catalytic performance for Mannich-type reactions due to the postfunctionalized V═O active sites.[18] Furthermore, porous VO(salen)-derived MOFs documented by Cui and co-workers allowed alcohol derivatives to be effectively catalyzed into the corresponding aldehydes with an elevated enantioselectivity and activity.[10] Moreover, the results reported by Farha and co-workers verified that 2-chloroethyl ethyl sulfide (CEES), a simulator of mustard gas, could be oxidized into an oxidized sulfoxide (CEESO) by VO_2-uploaded nanotubes.[11] Therefore, the modification of porous MOF platforms by implanting V═O units could realize the functionalization of the MOF materials and effectively improve the catalytic effect for specific chemical reactions. However, such related research has still scarcely been reported so far.

Inspired by the excellent catalytic performance devoted by previously documented porous VO-dock MOFs/COFs, we carried out a cation exchange by soaking $\{(Me_2NH_2)[Tm_3(HPTTBA)_2]\cdot 3DMF\cdot 3H_2O\}_n$ (**1-Tm**) units to form the blue crystalline material $\{(Me_2NH_2)_2[VO(H_2O)][Tm_2(BDCP)_2]\cdot 3DMF\cdot 3H_2O\}_n$ (**NUC-11**), whose structure could be verified by single-crystal X-ray diffraction analysis of the incompletely exchanged $\{(Me_2NH_2)_{1.5}[(VO(H_2O)_2)_{0.5}Tm_{0.5}][Tm_2(BDCP)_2]\cdot 3DMF\cdot 3H_2O\}_n$ (**NUC-11H**). In **NUC-11**, $[Tm_2(CO_2)_8]$ SBUs are connected by four deprotonated carboxyl groups of H_5BDCP to form a porous 3D host framework of $\{[Tm_2](BDCP)_2\}_n$. $[V^{IV}O(H_2O)_2]$ units are further decorated on the inner wall of the channels by two coordination covalent bonds formed from the remaining spare deprontoated carboxyl group of H_5BDCP, resulting in the targeted VO-docked MOFs with a void volume of 47.4%.

EXPERIMENTAL SECTION

Preparation of NUC-11. $\{(Me_2NH_2)[Tm_3(HPTTBA)_2]\cdot 3DMF\cdot 3H_2O\}_n$ (**1-Tm**) was prepared by employing a previously reported synthetic route.[36] A 0.1 g portion of freshly obtained single crystals of **1-Tm** was soaked in a solution of 0.1 g of $VOSO_4$, 8 mL of H_2O, and 2 mL of DMF for 5 days at 310 K. During the soaking period, the $VOSO_4$ solution was refreshed every day and the crystal sample was monitored with ICP. Unfortunately, only the partially prepared product (**NUC-11H**) could be characterized by single-crystal X-ray diffraction, which displayed that mononuclear Tm ions have been half-exchanged, in accordance with the data of ICP and elemental analysis. Anal. Calcd for the sample of **NUC-11H** suitable for single-crystal X-ray diffraction ($C_{127}H_{100}N_{10}O_{49}Tm_5V$): C, 44.27; H, 2.93; N, 4.06; Tm, 24.51; V, 1.48. Found: C, 44.12; H, 2.85; N, 3.97; Tm, 24.33; V, 1.55. IR (KBr pellet, cm^{-1}, Figure S2): 3417 (vs), 1613 (s), 1385 (s), 1250 (w), 1124 (s), 981 (s), 755 (w), 691 (w), 605 (w), 517 (w). The completely cation exchanged sample of **NUC-11** was obtained by cation exchange over 10 days with a Tm:V mole ratio of 2.02:1.00, as determined by ICP analysis.

Catalytic Cycloadditions of CO_2 with Various Epoxides. Typically, certain amounts of fully activated **NUC-11**, epoxide, and tetrabutylammonium bromide (Bu_4NBr) were employed and sealed in a 20 mL stainless-steel reactor equipped with a magnetic stirrer, and then the reactor was transferred into a constant-temperature water bath to reach the desired temperature. CO_2 was continuously purged into the reactor to manitain the desired pressure condition. After the reaction was over, the heterogeneous catalyst **NUC-11** could be easily collected by centrifugation separation and resued by washing with DMF and Cl_2CH_2 in turn. ^1H NMR spectroscopy and GC/MS were employed to determine the conversion rate and yield of the transformed product.

Catalytic Oxidation of 2-Chloroethyl Ethyl Sulfide. In a typical catalytic reaction, 50 mg of the catalyst (**NUC-11**) with 0.025 mmol of V═O active sites, 2.0 mmol of *tert*-butyl hydroperoxide, and 1 mmol of 2-chloroethyl ethyl sulfide were dispersed in a dram vial in the presence of 3 mL of acetonitrile. Then the vial was transferred to a water bath to reach the desired temperature. After completion of the reaction, the mixture was washed with DMF and reused for successive catalysis experiments. The desired product was determined by ^1H NMR spectroscopy and GC-MS analysis.

RESULTS AND DISCUSSION

Description of Crystal Structure. As judged by a single-crystal X-ray diffraction (SCXRD) analysis of **NUC-11H** and the metal elemental analysis of ICP, **NUC-11** crystallized in the monoclinic space group $C2/c$ with one crystallographically independent ion of Tm^{III}, one $V^{IV}O(H_2O)_2$, and half of $BDCP^{5-}$ being included in the asymmetric heterometallic unit. It is worth mentioning that the single-crystal transformation took place after cation exchange with cell parameters of a = 18.805 Å, b = 23.195 Å, and c = 21.192 Å being converted into a = 17.982 Å, b = 23.007 Å, and c = 21.643 Å. At the same time, H_6PTTBA was decarboxylated *in situ* to form the pentacarboxyl ligand H_5BDCP (Scheme 1). As demonstrated

Scheme 1. Cation Exchange Strategy for NUC-11 by an Impregnation Method

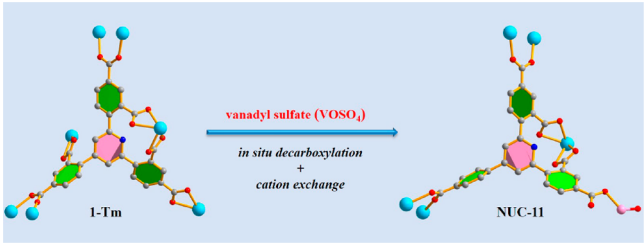

in Figure 1, three $\{Tm_2\}$ SBUs were connected by one $BDCP^{5-}$ to form the 3D host framework $\{[Tm_2](BDCP)_2\}_n$, which was further decorated by the cation $[VO(H_2O_2)]^{2+}$ to result in one anionic 3d−4f 3D heterometallic $[VO(H_2O)_2]_2[Tm_2]$-organic framework with 1D open channels. Such an anionic framework was further charge-balanced by the dimethylamine cation generated *in situ* by the decomposition of DMF molecules. Furthermore, to observe the IR spectrum shown in Figure S2, the strong adsorption peak at 981 cm^{-1} confirmed that terminal V═O stretches existed. Meanwhile, the valence of vanadium was confirmed by an XPS spectrum (Figure S4); characteristic binding energies at 524 and 517 eV were observed, consistent with V $2p_{3/2}$ and V $2p_{1/2}$, respectively, revealing that the oxidation state of vanadium in **NUC-11** was mainly +4.[31−34] The component ratio for V and

https://dx.doi.org/10.1021/acs.inorgchem.1c00053
Inorg. Chem. 2021, 60, 5005−5013

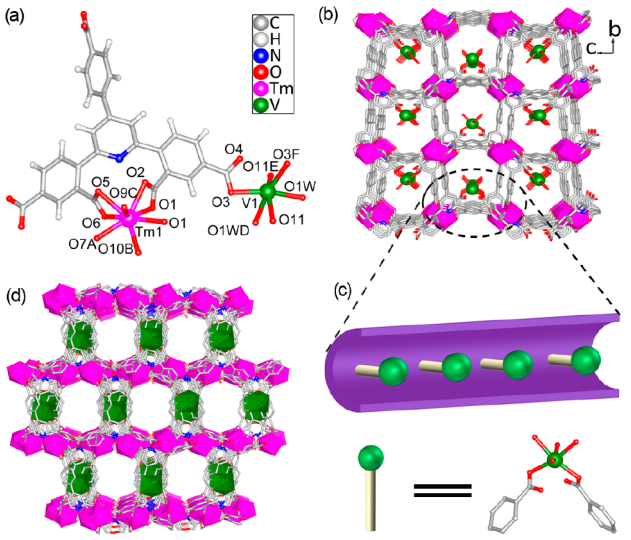

Figure 1. Coordination mode of Tm(III) and V(IV) ions: (a) the 3D framework and (b) schematic representation of (c) channels in **NUC-11** decorated with $[V^{IV}O(H_2O)_2]$ units (green, V; pink, Tm; red, O; blue, N, gray, C). (d) 3D channels containing the framework of **NUC-11** along the [1,0,−1] axis.

Tm obtained from an ICP determination was also consistent with the conclusion of SCXRD analysis.

Significantly, **NUC-11** represents the first example of a V═O modified porous MOF, in which carboxylic groups ($-CO_2H$) further grasp $[V^{IV}O(H_2O)_2]$ units on the initial basic skeleton along with the formation of covalent bonds as fixed ropes. So far, only Ma and co-workers have obtained several 2D VO-COFs synthesized from a postsynthetic modification with vanadyl acetylacetonate, which exhibited better catalytic performance due to its intrinsic features, including porous structures and V═O groups.[33] Moreover, from the aspect of structural modification, **NUC-11** shows great structural similarity with VO-COFs: that is, V═O groups exist in the form of a suspension on the inner wall of the channels. Thus, this work offers a feasible synthesis strategy for the functionalization of porous MOFs by postsynthesis modification, which could meet the needs of multidimensional skeleton links and further grasp targeted functional metal units at the same time.

As displayed in Figure 1a and Figure S1a, the Tm(III) ion was first chelated by two deprotonated α-carboxyl groups from two phenyl rings stationed on both sides of the $N_{pyridine}$ atom. Then two Tm(III) ions were further bridged by four γ-position μ_2-η^1:η^1 carboxyl groups subordinated to four phenyl rings, among which two were located at the 4-position of pyridine and other two at the 2-position of pyridine. Thus, eight carboxyl groups from six $BDCP^{5-}$ ligands synergistically connected two Tm(III) ions to form the basic spindle-shaped binuclear SBUs of $[Tm_2(CO_2)_8]$.

Furthermore, as dispalyed in Figure 1b, each ligand of $BDCP^{5-}$ with the assistance of four carboxyl groups could connect three $\{Tm_2\}$ SBUs to generate a 3D grid network featuring 1D channels with a window size of ca. 7.41 × 8.63 Å alongthe *a* axis. There was still one remaining carboxyl group for each BDCP ligand, which renders further modification feasible. Interestingly, V═O ions were grafted into the established host framwork of $\{[Tm_2](PTTBA)_2\}_n$ by coordinating to μ_1-η^1:η^0 carboxyl groups subordinated to two phenyl rings situated on the 6-position of pyridine from two neighboring BDCP ligands. Meanwhile, each vanadium was further coordinated by one aquous molecule except for one originally teminal oxygen atom (Figure 1b ,c). Undoubtedly, the successful docking of $[V^{IV}O(H_2O)_2]$ units could cause the steadiness of the host three-dimensional skeleton. Moreover, it is worth mentioning that the immobilized $[V^{IV}O(H_2O)_2]$ units were rightly situated in the regions of inner channel surfaces, which make **NUC-11** a potential heterogeneous catalyst for some specific organic reactions due to the fact that V═O could be taken as strong Lewis acid and base sites.[35−38] Meanwhile, as exhibited in Figure 1d, **NUC-11** had regular 1D channels of ca. 7.68 × 8.69 $Å^2$ along the [1,0,−1] axis. Finally, a topological analysis indicated that the whole structure of **NUC-11** could be defined as a (4,6)-connected network with the point symbol $\{6^2.5^3.6\}_2\{4^4.5^2.6^2.7^2.8^4.9\}$ by defining $BDCP^{5-}$ and $[Tm_2(CO_2)_8]$ SUBs as 4- and 6-connected nodes, respectively (Figure S1b).

Water Stability. Their low stability especially in an aqueous environment and deliquescence during preservation have caused MOFs to be scarcely popularized in practical applications.[35] Consequently, to test the water stability of the cation-exchanged framework of **NUC-11**, several simulated aquatic systems at different temperatures were employed for soaking the **NUC-11** crystals. After a certain time, the crystals were separated by centrifugal filtration and the structures determined by a PXRD analysis. As shown in Figure S5, whether in normal temperature water or boiling water, PXRD patterns corresponded to that the pattern of the as-synthesized **NUC-11**, implying the strong water tolerance of **NUC-11**. The reason for strong water stability is mainly that the modified V═O ions may influence the pore environment and build a strong hydrophobic inner surface of **NUC-11**.[36]

Gas Adsorption Studies. In view of the total solvent-accessible volume of 47.4% for **NUC-11** derived from PLATON software, the permanent porosity was checked by a cryogenic nitrogen sorption experiment on the fully activated sample (Figure S6), which was obtained by the manipulation of solvent exchange and evacuation at 150 °C for 6 h. As shown in Figure S7, the N_2 sorption isotherms at 77 K presented a typical reversible type I sorption behavior. The increaseing adsorption capacity in the low-pressure region confirmed that **NUC-11** had microporous characteristics.[37,38,39] With an increase in pressure, the N_2 uptake gradually tended to be saturated, giving a maximum adsorption quantity of 325 cm^3 (STP) g^{-1} at 1 atm with the Langmuir and BET specific surface areas being 1547.8 and 1326.4 m^2 g^{-1}, respectively.

Prior to carrying out the catalytic cycloaddition of CO_2, the sorption performance for CO_2 was determined, as illustrated in Figure 2. The adsorption quantity (1 bar) of CO_2 reached 98.3 and 66.4 cm^3 g^{-1} at 273 and 298 K, respectively, which was better than documented heterometallic doping MOFs with approximate porosity.[39] which should be ascribed to the contribution from $[V^{IV}O(H_2O)_2]$ units. Meanwhile, the CO_2 isosteric heat (Q_{st}) was calculated by virial method based on the CO_2 isotherms measured at 273 and 293 K, from which the resulted Q_{st} value was 26.75 kJ mol^{-1} at zero loading and 24.92 kJ mol^{-1} at the maximum measured loading (Figure S8). Furthermore, with CO_2 loading, no obvious change in the Q_{st} value was observed, indicating that the binding sites were homogeneous. Moreover, it is worth noting that the extremely high isosteric heat value was probably caused by the additional contribution of vanadium ions with significant π back-bonding,

https://dx.doi.org/10.1021/acs.inorgchem.1c00053
Inorg. Chem. 2021, 60, 5005−5013

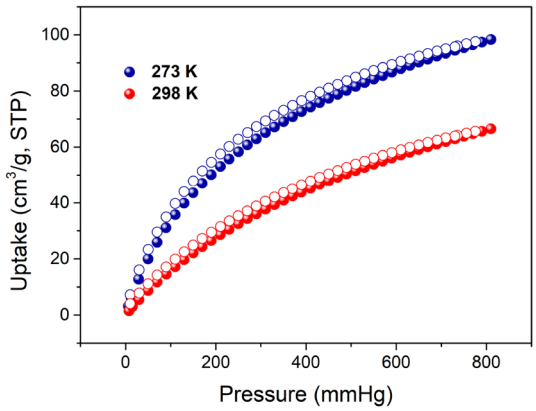

Figure 2. CO_2 adsorption isotherms at 273 and 298 K.

which gave **NUC-11** an excellent potential separation performance for mixed gases, just as was documented for **VMOF-74**.[39,40]

Catalytic Cycloaddition of CO_2 and Epoxides. In view of these remarkable characteristics of **NUC-11**, including a high proportion of void volume, a large specific surface area, abundant active metal sites (V═O and Tm^{III}), and moderate CO_2 adsorption capacity, the catalytic activity of **NUC-11** was explored for the cycloaddition reaction of epoxides with CO_2, widely regarded as a two-step catalytic reaction.[40−52] To explore the influence the of reaction conditions on the conversion rate of epoxide, propylene oxide was selected as a model substrate and the desired product of propylene carbonate was determined by ^{1}H NMR (Figure S12). In a typical experiment, the amount of propylene oxide was fixed at 20 mmol, exhibiting a low conversion rate of 9% in the presence of only activated **NUC-11** at 50 °C (entry 2, Table 1); meanwhile a similarly low conversion rate of 17% was observed in the presence of only the cocatalyst Bu_4NBr (entry 3). However, by simultaneously employing 50 mg of **NUC-11** and 2.5% Bu_4NBr, the yield could reach 44%, as shown in entry 4. On the other hand, the almost stagnant coupling reaction of entry 1 indicates that **NUC-11** and Bu_4NBr with thier unique superiorities work on different steps for the second-order coupling reaction. Furthermore, with an increase in the reaction temperature from 50 to 70 °C (entries 4−6), the conversion rate accordingly increased, showing that temperature is an important factor to influence the catalytic efficency. However, when the quantity of Bu_4NBr as cocatalyst was doubled, the conversion rate could quickly increase to 99% at 70 °C within 6 h. Therefore, the optimal conditions were defined as 50 mg of **NUC-11**, 5 mol % of Bu_4NBr, 70 °C, and 6 h. In addition, when the catalyst dose was doubled, a high reaction yield could be obtained within 4 h (entry 10). To better understand the synergistic effect of the various active species in **NUC-11**, some blank experiments in the presence of raw materials including $Tm(NO_3)_3$, $VOSO_4$, and H_5BDCP ligand as single catalysts were carried out under the optimal conditions. As shown in Table S4, the catalytic activities of these compounds were lower than that **NUC-11**.

Furthermore, a series of epoxide derivatives with different substitutes and molecular sizes were used to explore the effect of substituents on the reaction and the catalytic universality of **NUC-11** under the established optimal reaction conditions, in which the molecular sizes of these epoxide derivatives were all smaller than the pore diameter of **NUC-11** to avoid a surface catalysis (Table S3). Just as expected, all of the epoxide derivatives could be successfully transformed into the corresponding carbonates with high conversion rate of above 93%, as demonstrated in Table 2; the corresponding ^{1}H NMR spectra of products are given in Figures S13−S16. With regard to the difference in catalytic efficienciesa, entries 1−4 exhibit a higher conversion rate in comparison to entry 5; a similar

Table 1. Cycloaddition Reaction of CO_2 with 1,2-Epoxypropane under Various Conditions[a]

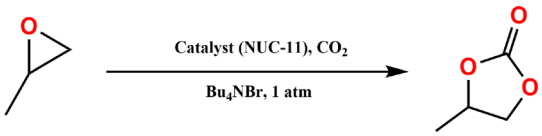

entry	NUC-11 (mg)	Bu_4NBr (mol %)	T (°C)	time (h)	yield (%)[b]
1	0	0	50	6	<1
2	50	0	50	6	9
3	0	2.5	50	6	17
4	50	2.5	50	6	44
5	50	2.5	60	6	60
6	50	2.5	70	6	75
7	50	5	50	6	58
8	50	5	60	6	81
9	50	5	70	6	99
10	100	5	70	4	99

[a]Reaction conditions: 1,2-epoxypropane (20 mmol), **NUC-11** (50 mg, containing 0.025 mmol of V═O ions), solvent free, CO_2 (1 atm), 6 h. [b]Checked by ^{1}H NMR and GC-MS spectroscopy with *n*-dodecane as the internal standard.

Table 2. Cycloaddition Reaction of CO_2 and Various Epoxides with NUC-11 as Catalyst[a]

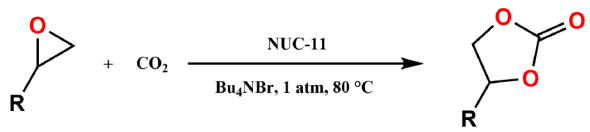

Entry	Epoxides	Products	Yield (%)[b]	TON[c]
1		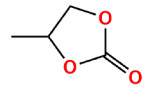	99	3960
2	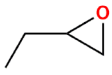	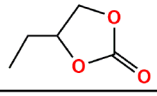	98	3920
3	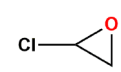	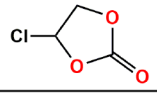	99	3960
4	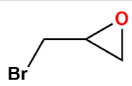	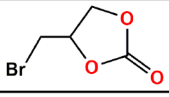	99	3960
5	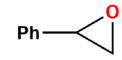	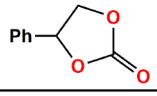	93	3720

[a]Reaction conditions: substrate (20 mmol), Bu_4NBr (5 mol %), **NUC-11** (50 mg, 0.025 mol %, based on the V═O ions), CO_2 (1 atm), 70 °C, 6 h. [b]Determined by GC/MS with *n*-dodecane as the internal standard. [c]TON (turnover number) = (mol of product)/(mol of catalyst).

https://dx.doi.org/10.1021/acs.inorgchem.1c00053
Inorg. Chem. 2021, 60, 5005−5013

phenomenon has been found in other documented MOF-based catalysts.[48−55] From our speculation, the reasons include mainly (i) epoxide derivatives with a large molecular size will affect their accessibility into the nanochannels and (ii) large substituents on the epoxides with strong steric hindrance will influence the opportunity to contact with catalytically active sites. Moreover, in comparison to the previously reported monometallic Ln-organic framework,[49−53] cation-exchanged **NUC-11** exhibited a faster catalytic efficiency. The reason for this, structurally, is thaat the postmodified $[V^{IV}O(H_2O)_2]$ units on the surface of the nanochannels protrude into the position where the substrates could be easily hit, and hence an improved catalytic efficiency could be realized.

Moreover, recycling experiments using 20 mmol of propylene oxide as the substrate and 50 mg of **NUC-11** as the catalyst were repeated five times under the optimal conditions. After each cycle, the **NUC-11** sample was recovered by simple filtration and washing with DMF. As shown in Figure S10, the transformation yield after 6 h is almost unchanged within five cycles, which might be interpreted as the catalytic continuity of **NUC-11**. An inductively coupled plasma (ICP) analysis demonstrated that only trace amounts of Tm(III) (∼0.012%) and V(IV) (∼0.014%) ions were monitored form the filtrate, which ruled out the leaching of active species in the process of the catalytic cycloaddition reaction. Such a result was reinforced by the PXRD pattern of recovered **NUC-11** shown inFigure S9; the fine parallelism with the result of the original catalyst confirmed the excellent reusability of **NUC-11**. Meanwhile, a 10-fold amplification reaction by using 500 mg of the catalyst was simultaneously carried out under the optimal conditions, as shown in Figure S11. As a result, **NUC-11** still had high catalytic efficiency after five cycles, indicating that **NUC-11** possessed excellent practical application prospects.

The proposed mechanism of chemical cycloaddition of alkyl epoxides with CO_2 into carbonates is given in Figure 3. First, substrate molecules of the epoxide dispersed in the nano-channels were expeditiously polarized by protruding V═O ions in the pore wall. Subsequently, the bromine ion released from Bu_4NBr makes a nucleophilic attack on the α-carbon atom of epoxide, leaving an instantaneous anionic intermediate of a bromoalkoxide that coordinated weakly with the V═O ions. Furthermore, the bromoalkoxide undergoes a nucleophilic addition with the CO_2 molecules polarized by Lewis acidic sites to form the alkylcarbonate anion. Ultimately, the transformation of the alkylcarbonate anion into the five-membered-ring carbonate is accomplished by a closed-loop step.[52−55]

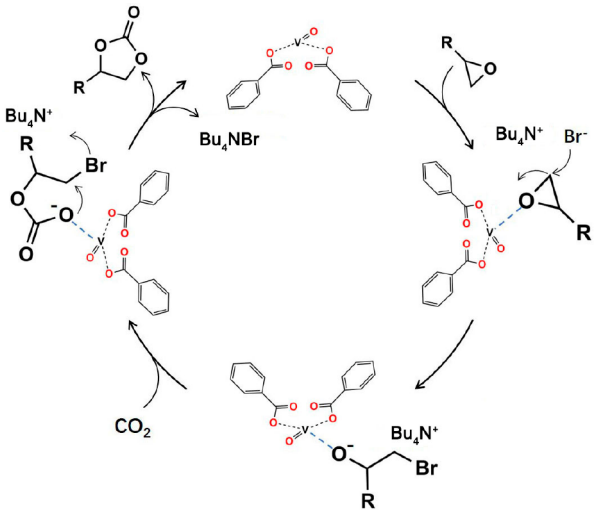

Figure 3. Representation of the possible mechanism of cycloaddition of epoxide with CO_2.

Catalytic Oxidation of 2-Chloroethyl Ethyl Sulfide. In addition to the chemical fixation of CO_2, the catalytic efficiency of **NUC-11** for oxidizing a simulator of mustard gas, 2-chloroethyl ethyl sulfide (CEES), was checked by employing a 70% aqueous solution of *tert*-butyl hydroperoxide (TBHP) with acetonitrile as the solvent during the experiments. The results summarized in Table 3 show that **NUC-11** possesses an ideal catalytic performance, which is enhanced with an increase in the time and temperature. The conversion rate at 25 °C varied from 58% to 99% with time from 1 to 4 h, whereas the conversion rate could reach almost 100% within 2 h when the reaction temperature was set at 40 °C. It is worth mentioning that the conversion rate is one more important indicator that reflects the transformation of mustard gas into low-toxicity products of oxidized sulfoxide (CEESO).[56−69] Furthermore, blank experiments employing 0.025 mmol of the related raw materials of **NUC-11** were conducted at 40 °C over 2 h, as detailed in Table S5. The dramatically decreased conversion rate implied that the synergistic effect of various active species exists in **NUC-11**.

Table 3. Oxidation of CEES into CEESO under Different Conditions[a]

entry	catalyst **NUC-11** (mg)	T (°C)	time (h)	conversion (%)[b]	yield (%)[b]
1	50	25	1	58	71
2	50	25	2	73	74
3	50	25	3	89	85
4	50	25	4	99	89
5	50	30	3	99	94
6	50	40	2	99	92

[a]Reaction conditions: catalyst (**NUC-11**) 50 mg (containing 0.025 mmol of vanadium), CEES (1 mmol), TBHP (2.0 mmol), acetonitrile 3 mL, 100 rpm. [b]Determined by GC/MS with *n*-dodecane as the internal standard.

On the basis of the structural features of **NUC-11** and previous documentation by Ma,[18] the mechanism of catalytic oxidation of 2-chloroethyl ethyl sulfide was speculated and is displayed in Figure 4. First, the active Lewis acid sites of V═O units offered a charge attraction to the oxygen atom of TBHP and then formed weak coordination bonds along with the V═O double bond being opened, generating the intermediate of oxygenated compounds. Second, the instantaneous intermediate made an nucleophilic attack to the sulfur atom of the approaching 2-chloroethyl ethyl sulfide concentrated in the 1D channels of **NUC-11**, consequently achieving the purpose of synergetic oxygen transfer along with the catalyst recovery.

Remarkably, it is worth noting that **NUC-11** exhibited a better catalytic efficiency in comparison to the documented VO-COFs, which may be ascribed to the combination of separate 4f $[Tm_2(CO_2)_8]$ SBUs and 3d $[V^{IV}O(H_2O)_2]$ units. In VO-COFs, only VO units could act as the active centers to take part in the reaction process, just as was elaborated in the mechanism detailed above. However, in addition the highly

https://dx.doi.org/10.1021/acs.inorgchem.1c00053
Inorg. Chem. 2021, 60, 5005−5013

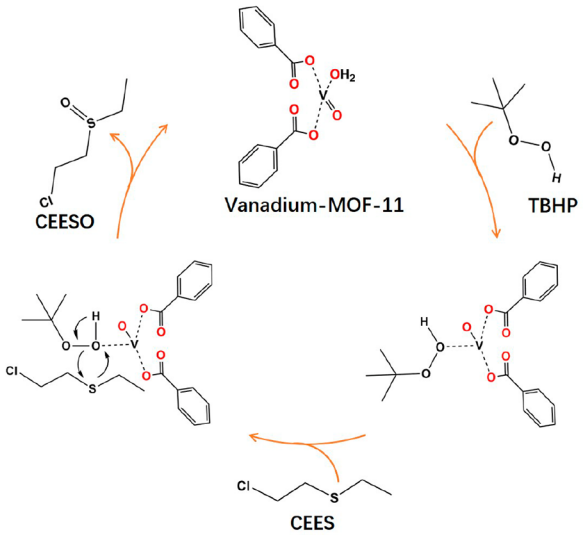

Figure 4. Proposed catalytic mechanism of **NUC-11**-catalyzed sulfide oxidation.

active V═O units discussed in detail for the catalytic reaction mechanism, **NUC-11** also contained high-coordination-number Tm^{3+} ions, which could tend to coordinate with TBHP due to the fact that the abundant hybrid orbitals $f^n d^{2+m} sp^3$ around Tm^{3+} ions give it a wide coordination number range. Furthermore, to some extent, both the chemical fixation of CO_2 and the oxidation reaction had an approximate reaction mechanism, during which the formation of coordination intermediates existed.

Just as was emphasized for the chemical fixation of CO_2, the recoverability and sustained stability of an emerging catalyst are requirements that must be met before industrial consideration of applications, which encouraged us to carry out cyclic oxidization experiments on the **NUC-11** catalyst. After each test, the sample of **NUC-11** was collected by centrifugal separation and then rinsed three times with methanol to remove the substrates. Consequently, the obtained **NUC-11** sample was immersed in acetone for 10 min, which was easily evaporated after vacuum drying. As displayed in Figure S17, the conversion rate in the presence of the recycled **NUC-11** catalyst did not change significantly, which verified that the V═O docked MOFs of **NUC-11** could be viewed as one potential candidate for destroying mustard gas. Meanwhile, the recycled **NUC-11** sample was checked by PXRD, which exhibited that the characteristic peaks could be well fitted with those of the original crystalline sample, as shown in Figure S9. The amounts of leached homogeneous Tm(III) and V(IV) species were only 0.009% and 0.013%, respectively, in the filtered liquor as monitored by ICP analysis, verifying that a realistic heterogeneous catalytic process was feasible.

■ CONCLUSIONS

By cation exchange, V═O units were successfully docked on the channel inner walls in the basic porous framwork of **1-Tm** as precursors to generate the novel functional porous heterometallic-organic framework $\{[VO(H_2O)]\text{-}[Tm_2(BDCP)_2]\}_n$, which displayed excellent catalytic performance for the chemical synthesis of carbonates from related epoxides and CO_2 with a high conversion rate. In addition, a simulator of mustard gas, 2-chloroethyl ethyl sulfide, could be quickly and efficiently oxidized into low-toxicity products of oxidized sulfoxide by *tert*-butyl hydroperoxide in the presence of the **NUC-11** catalyst. Thus, this study offers a new method for the design and synthesis of functional-unit-modified porous MOFs by postsynthesis modification.

■ ASSOCIATED CONTENT

Supporting Information

The Supporting Information is available free of charge at https://pubs.acs.org/doi/10.1021/acs.inorgchem.1c00053.

Crystallographic data and refinement parameters of **NUC-11**, selected bond lengths and angles, TGA curves of as-synthesized (black) and activated (red) samples of **NUC-11**, PXRD patterns of **NUC-11** after water treatment, IR spectra, and N_2 absorption/desorption isotherms of **NUC-11** at 77 K (PDF)

Accession Codes

CCDC 2015095 contains the supplementary crystallographic data for this paper. These data can be obtained free of charge via www.ccdc.cam.ac.uk/data_request/cif, or by emailing data_request@ccdc.cam.ac.uk, or by contacting The Cambridge Crystallographic Data Centre, 12 Union Road, Cambridge CB2 1EZ, UK; fax: +44 1223 336033.

■ AUTHOR INFORMATION

Corresponding Author

Xiutang Zhang − *Department of Chemistry, College of Science, North University of China, Taiyuan 030051, People's Republic of China;* orcid.org/0000-0002-5654-7510; Email: xiutangzhang@163.com

Authors

Hongtai Chen − *Department of Chemistry, College of Science, North University of China, Taiyuan 030051, People's Republic of China*

Liming Fan − *Department of Chemistry, College of Science, North University of China, Taiyuan 030051, People's Republic of China;* orcid.org/0000-0003-4615-0533

Tuoping Hu − *Department of Chemistry, College of Science, North University of China, Taiyuan 030051, People's Republic of China;* orcid.org/0000-0001-7437-3246

Complete contact information is available at: https://pubs.acs.org/10.1021/acs.inorgchem.1c00053

Notes

The authors declare no competing financial interest.

■ ACKNOWLEDGMENTS

This work received financial support from the Natural Science Foundation of China (21101097, 21801230) and the Opening Foundation of Key Laboratory of Laser & Infrared System of Shandong University (2019-LISKFJJ-005).

■ REFERENCES

(1) Feng, L.; Wang, K.-Y.; Lv, X.-L.; Yan, T.-H.; Li, J.-R.; Zhou, H.-C. Modular Total Synthesis in Reticular Chemistry. *J. Am. Chem. Soc.* **2020**, *142*, 3069−3076.

(2) Yuan, S.; Huang, L.; Huang, Z.; Sun, D.; Qin, J.-S.; Feng, L.; Li, J.; Zou, X.; Cagin, T.; Zhou, H.-C. Continuous Variation of Lattice Dimensions and Pore Sizes in Metal-Organic Frameworks. *J. Am. Chem. Soc.* **2020**, *142*, 4732−4738.

(3) Howlader, P.; Zangrando, E.; Mukherjee, P. S. Self-Assembly of Enantiopure Pd12 Tetrahedral Homochiral Nanocages with Tetrazole Linkers and Chiral Recognition. *J. Am. Chem. Soc.* **2020**, *142*, 9070−9078.
(4) Mondal, B.; Mukherjee, P. S. Cage Encapsulated Gold Nanoparticles as Heterogeneous Photocatalyst for Facile and Selective Reduction of Nitroarenes to Azo Compounds. *J. Am. Chem. Soc.* **2018**, *140*, 12592−12601.
(5) Howlader, P.; Mondal, B.; Purba, P. C.; Zangrando, E.; Mukherjee, P. S. Self-Assembled Pd(II) Barrels as Containers for Transient Merocyanine Form and Reverse Thermochromism of Spiropyran. *J. Am. Chem. Soc.* **2018**, *140*, 7952−7960.
(6) Rosen, A. S.; Mian, M. R.; Islamoglu, T.; Chen, H.; Farha, O. K.; Notestein, J. M.; Snurr, R. Q. Tuning the Redox Activity of Metal-Organic Frameworks for Enhanced, Selective O_2 Binding: Design Rules and Ambient Temperature O_2 Chemisorption in a Cobalt-Triazolate Framework. *J. Am. Chem. Soc.* **2020**, *142*, 4317−4328.
(7) Islamoglu, T.; Chen, Z.; Wasson, M. C.; Buru, C. T.; Kirlikovali, K. O.; Afrin, U.; Mian, M. R.; Farha, O. K. Metal-Organic Frameworks Against Toxic Chemicals. *Chem. Rev.* **2020**, *120* (16), 8130−8160.
(8) Wang, H.; Qian, C.; Liu, J.; Zeng, Y.; Wang, D.; Zhou, W.; Gu, L.; Wu, H.; Liu, G.; Zhao, Y. Integrating Suitable Linkage of Covalent Organic Frameworks into Covalently Bridged Inorganic/Organic Hybrids Toward Efficient Photocatalysis. *J. Am. Chem. Soc.* **2020**, *142*, 4862−4871.
(9) Idrees, K. B.; Chen, Z.; Zhang, X.; Mian, M. R.; Drout, R. J.; Islamoglu, T.; Farha, O. K. Tailoring Pore Aperture and Structural Defects in Zirconium-Based Metal-Organic Frameworks for Krypton/Xenon Separation. *Chem. Mater.* **2020**, *32*, 3776−3782.
(10) Xi, W.; Liu, Y.; Xia, Q.; Li, Z.; Cui, Y. Direct and Post-Synthesis Incorporation of Chiral Metallosalen Catalysts into Metal-Organic Frameworks for Asymmetric Organic Transformations. *Chem. - Eur. J.* **2015**, *21*, 12581−12585.
(11) Buru, C. T.; Wasson, M. C.; Farha, O. K. $H_5PV_2Mo_{10}O_{40}$ Polyoxometalate Encapsulated in NU-1000 Metal-Organic Framework for Aerobic Oxidation of a Mustard Gas Simulant. *ACS Appl. Nano Mater.* **2020**, *3*, 658−664.
(12) Kirlikovali, K. O.; Chen, Z.; Islamoglu, T.; Hupp, J. T.; Farha, O. K. Zirconium-Based Metal-Organic Frameworks for the Catalytic Hydrolysis of Organophosphorus Nerve Agents. *ACS Appl. Mater. Interfaces* **2020**, *12*, 14702−14720.
(13) Liu, J.; Zhao, Y.; Dang, L. L.; Yang, G. P.; Ma, L. F.; Li, D. S.; Wang, Y. Y. Highly stable 3D porous HMOF with enhanced catalysis and fine color regulation by the combination of d- and p-ions when compared with those of its monometallic MOFs. *Chem. Commun.* **2020**, *56* (62), 8758−8761.
(14) Wu, Y. P.; Tian, J. W.; Liu, S.; Li, B.; Zhao, J.; Ma, L. F.; Li, D. S.; Lan, Y. Q.; Bu, X. Bi-Microporous Metal-organic-frameworks with Cubane $[M_4(OH)_4]$ (M = Ni, Co) Clusters and Pore Space Partition for Electrocatalytic Methanol Oxidation Reaction. *Angew. Chem., Int. Ed.* **2019**, *58*, 12185−12189.
(15) Huang, D.; Wu, X.; Tian, J.; Wang, X.; Zhou, Z.; Li, D. Assembling of a novel 3D Ag(I)-MOFs with mixed ligands tactics: Syntheses, crystal structure and catalytic degradation of nitrophenol. *Chin. Chem. Lett.* **2018**, *29*, 845−848.
(16) Qin, Z.; Dong, W.; Zhao, J.; Wu, Y.; Zhang, Q.; Li, D. A water-stable Tb(III)-based metal-organic gel (MOG) for detection of antibiotics and explosives. *Inorg. Chem. Front.* **2018**, *5*, 120−126.
(17) Wu, Y.; Zhou, W.; Zhao, J.; Dong, W.; Lan, Y.; L, D.; Sun, C.; Bu, X. Surfactant-assisted phase-selective synthesis of new cobalt MOFs and their efficient electrocatalytic hydrogen evolution reaction. *Angew. Chem., Int. Ed.* **2017**, *56*, 13001−13005.
(18) Vardhan, H.; Verma, G.; Ramani, S.; Nafady, A.; Al-Enizi, A. M.; Pan, Y.; Yang, Z.; Yang, H.; Ma, S. Covalent Organic Framework Decorated with Vanadium as a New Platform for Prins Reaction and Sulfide Oxidation. *ACS Appl. Mater. Interfaces* **2019**, *11*, 3070−3079.
(19) Wang, X.; Liu, J.; Zhang, L.; Dong, L.; Li, S.; Kan, Y.; Li, D.; Lan, Y. Monometallic catalytic models hosted in stable metal-organic frameworks for tunable CO_2 photoreduction. *ACS Catal.* **2019**, *9*, 1726−1732.
(20) Wei, J.-H.; Yi, J.-W.; Han, M.-L.; Li, B.; Liu, S.; Wu, Y.-P.; Ma, L.-F.; Li, D.-S. A Water-Stable Terbium(III)-Organic Framework as a Chemosensor for Inorganic Ions, Nitro-Containing Compounds and Antibioticsin Aqueous Solutions. *Chem. - Asian J.* **2019**, *14*, 3694−3701.
(21) Tian, J.-W.; Wu, Y.-P.; Li, Y.-S.; Wei, J.-H.; Yi, J.-W.; Li, S.; Zhao, J.; Li, D.-S. Integration of Semiconductor Oxide and a Microporous (3,10)-Connected Co_6-Based Metal-Organic Framework for Enhanced Oxygen Evolution Reaction. *Inorg. Chem.* **2019**, *58*, 5837−5843.
(22) Wang, X.; Li, B.; Wu, Y.-P.; Tsamis, A.; Yu, H.-G.; Liu, S.; Zhao, Y.; Li, Y.-S.; Li, D.-S. Investigation on the Component Evolution of a Tetranuclear Nickel-Cluster-Based Metal-Organic Framework in an Electrochemical Oxidation Reaction. *Inorg. Chem.* **2020**, *59*, 4764−4771.
(23) Yu, C.-X.; Wang, K.-Z.; Li, X.-J.; Liu, D.; Ma, L.-F.; Liu, L.-L. Highly Efficient and Facile Removal of Pb^{2+} from Water by Using a Negatively Charged Azoxy-Functionalized Metal-Organic Framework. *Cryst. Growth Des.* **2020**, *20* (8), 5251−5260.
(24) Yang, X. G.; Zhai, Z. M.; Ma, L. F.; Yan, D. P. Fast Crystallization-Deposition of Orderly Molecule Level Heterojunction Thin Films Showing Tunable Up-Conversion and Ultrahigh Photoelectric Response. *ACS Cent. Sci.* **2020**, *6*, 1169−1178.
(25) Fu, H. R.; Wang, N.; Wu, X. X.; Li, F. F.; Zhao, Y.; Ma, L. F.; Du, M. Circularly Polarized Room-Temperature Phosphorescence and Encapsulation Engineering for MOF-Based Fluorescent/Phosphorescent WLEDs. *Adv. Optical Mater.* **2020**, *8* (13), 2000330.
(26) Yu, C. X.; Hu, F. L.; Song, J. G.; Zhang, J. L.; Liu, S. S.; Wang, B. X.; Meng, H.; Liu, L. L.; Ma, L. F. Ultrathin two-dimensional metal-organic framework nanosheets decorated with tetra-pyridyl calix [4] arene: Design, synthesis and application in pesticide detection. *Sens. Actuators, B* **2020**, *310*, 127819.
(27) Liu, J.; Yang, G. P.; Jin, J.; Wu, D.; Ma, L. F.; Wang, Y. Y. A first new porous d-p HMOF material with multiple active sites for excellent CO_2 capture and catalysis. *Chem. Commun.* **2020**, *56* (16), 2395−2398.
(28) Zhao, Y.; Wang, Y. J.; Wang, N.; Zheng, P.; Fu, H. R.; Han, M. L.; Ma, L. F.; Wang, L. Y. Tetraphenylethylene-Decorated Metal-Organic Frameworks as Energy-Transfer Platform for the Detection of Nitro-Antibiotics and White-Light Emission. *Inorg. Chem.* **2019**, *58*, 12700−12706.
(29) Wu, Y. P.; Tian, J. W.; Liu, S.; Li, B.; Zhao, J.; Ma, L. F.; Li, D. S.; Lan, Y. Q.; Bu, X. Bi-Microporous Metal-organic-frameworks with Cubane $[M_4(OH)_4]$ (M = Ni, Co) Clusters and Pore Space Partition for Electrocatalytic Methanol Oxidation Reaction. *Angew. Chem., Int. Ed.* **2019**, *58*, 12185−12189.
(30) Zhao, Y.; Yang, X. G.; Lu, X. M.; Yang, C. D.; Fan, N. N.; Yang, Z. T.; Wang, L. Y.; Ma, L. F. $\{Zn_6\}$ Cluster based metal-organic framework with enhanced room-temperature phosphorescence and optoelectronic performances. *Inorg. Chem.* **2019**, *58*, 6215−6221.
(31) Cheng, Y. J.; Wang, R.; Wang, S.; Xi, X. J.; Ma, L. F.; Zang, S. Q. Encapsulating $[Mo_3S_{13}]^{2-}$ clusters in cationic covalent organic frameworks: enhancing stability and recyclability by converting a homogeneous photocatalyst to a heterogeneous photocatalyst. *Chem. Commun.* **2018**, *54*, 13563−13566.
(32) Liu, F.-L.; Kozlevčar, B.; Strauch, P.; Zhuang, G.-L.; Guo, L.-Y.; Wang, Z.; Sun, D. Robust Cluster Building Unit: Icosanuclear Heteropolyoxocopperate Templated by Carbonate. *Chem. - Eur. J.* **2015**, *21* (51), 18847−18854.
(33) Wang, X.-P.; Chen, W.-M.; Qi, H.; Li, X.-Y.; Rajnák, C.; Feng, Z.-Y.; Kurmoo, M.; Boča, R.; Jia, C.-J.; Tung, C.-H.; Sun, D. Solvent-Controlled Phase Transition of a Co^{II}-Organic Framework: From Achiral to Chiral and Two to Three Dimensions. *Chem. - Eur. J.* **2017**, *23* (33), 7990−7996.
(34) Wang, Z.; Li, X. Y.; Liu, L. W.; Yu, S. Q.; Feng, Z. Y.; Tung, C. H.; Sun, D. Beyond Clusters: Supramolecular Networks Self-

Assembled from Nanosized Silver Clusters and Inorganic Anions. *Chem. - Eur. J.* **2016**, *22* (20), 6830−6836.
(35) Xu, Z.; Han, L.-L.; Zhuang, G.-L.; Bai, J.; Sun, D. In Situ Construction of Three Anion-Dependent Cu(I) Coordination Networks as Promising Heterogeneous Catalysts for Azide-Alkyne "Click" Reactions. *Inorg. Chem.* **2015**, *54* (10), 4737−4743.
(36) Yan, Z.-H.; Li, X.-Y.; Liu, L.-W.; Yu, S.-Q.; Wang, X.-P.; Sun, D. Single-Crystal to Single-Crystal Phase Transition and Segmented Thermochromic Luminescence in a Dynamic 3D Interpenetrated Ag-I Coordination Network. *Inorg. Chem.* **2016**, *55* (3), 1096−1101.
(37) Yuan, Y.; Sheng, K.; Zeng, S.; Han, X.; Sun, L.; Lončarić, I.; Zhan, W.; Sun, D. Engineering Cu/TiO_2@N-Doped C Interfaces Derived from an Atom-Precise Heterometallic $Cu^{II}_4Ti^{IV}_5$ Cluster for Efficient Photocatalytic Hydrogen Evolution. *Inorg. Chem.* **2020**, *59*, 5456−5462.
(38) Liu, Y.-N.; Hou, J.-L.; Wang, Z.; Gupta, R. K.; Jagličić, Z.; Jagodič, M.; Wang, W.-G.; Tung, C.-H.; Sun, D. An Octanuclear Cobalt Cluster Protected by Macrocyclic Ligand: In Situ Ligand-Transformation-Assisted Assembly and Single-Molecule Magnet Behavior. *Inorg. Chem.* **2020**, *59*, 5683−5693.
(39) Yu, F.; Ji, B.-Q.; Jagodič, M.; Su, Y.-M.; Zhang, S.-S.; Feng, L.; Kurmoo, M.; Jagličić, Z.; Sun, D. Copper(II)-Assisted Ligand Fragmentation Leading to Three Families of Metallamacrocycle. *Inorg. Chem.* **2020**, *59*, 13524−13532.
(40) Liang, X.-Q.; Gupta, R.-K.; Li, Y.-W.; Ma, H.-Y.; Gao, L.-N.; Tung, C.-H.; Sun, D. Structural Diversity of Copper(I) Cluster-Based Coordination Polymers with Pyrazine-2-thiol Ligand. *Inorg. Chem.* **2020**, *59*, 2680−2688.
(41) Ma, C.; Wang, P.; Liu, Z.; Xin, C.; Wang, S.; Jia, J.; Ma, P.; Niu, J.; Wang, J. Oxyfunctionalization of Alkanes Based on a Tricobalt(II)-Substituted Dawson-Type Rhenium Carbonyl Derivative as Catalyst. *Inorg. Chem.* **2020**, *59*, 8690−8698.
(42) Liang, Z.; He, Y.; Qiao, Y.; Ma, P.; Niu, J.; Wang, J. Sandwich-Type Heteropolyniobate Templated by Mixed Heteroanions. *Inorg. Chem.* **2020**, *59*, 7895−7899.
(43) Xu, Q.; Xu, B.; Kong, H.; He, P.; Wang, J.; Kannan, T.; Ma, P.; Wang, J.; Niu, J. Synthesis and Characterization of a Crown-Shaped 36-Molybdate Cluster and Application in Catalyzing Knoevenagel Condensation. *Inorg. Chem.* **2020**, *59*, 10665−10672.
(44) Zhang, M.; Liu, B.; Zhang, H.; Zhang, C.; Wang, J.; Niu, J. Synthesis and Mechanism Studies of a High-Nuclear $Mn_{72}W_{48}$ Cluster. *Inorg. Chem.* **2020**, *59*, 13733−13740.
(45) Li, D.; Ma, X.; Wang, Q.; Ma, P.; Niu, J.; Wang, J. Copper-Containing Polyoxometalate-Based Metal-Organic Frameworks as Highly Efficient Heterogeneous Catalysts toward Selective Oxidation of Alkylbenzenes. *Inorg. Chem.* **2019**, *58*, 15832−15840.
(46) Singh, V.; Liu, S.; Ma, P.; Drew, M. G. B.; Wang, J.; Niu, J. Versatile {Cp_2Ti} Grafted Hetero-Polyoxotungstate Clusters: Synthesis, Crystal Structure, and Photocurrent Properties. *Inorg. Chem.* **2020**, *59*, 1125−1136.
(47) He, J.; Li, J.; Han, Q.; Si, C.; Niu, G.; Li, M.; Wang, J.; Niu, J. Photoactive Metal-Organic Framework for the Reduction of Aryl Halides by the Synergistic Effect of Consecutive Photoinduced Electron-Transfer and Hydrogen-Atom-Transfer Processes. *ACS Appl. Mater. Interfaces* **2020**, *12*, 2199−2206.
(48) Sun, N.; Wang, C.; Wang, H.; Gao, X.; Jiang, J. Photonic Switching Porous Organic Polymers toward Reversible Control of Heterogeneous Photocatalysis. *ACS Appl. Mater. Interfaces* **2020**, *12*, 56491.
(49) Han, B.; Wang, H.; Wang, C.; Wu, H.; Zhou, W.; Chen, B.; Jiang, J. Postsynthetic Metalation of a Robust Hydrogen-Bonded Organic Framework for Heterogeneous Catalysis. *J. Am. Chem. Soc.* **2019**, *141*, 8737−8740.
(50) Liu, W.; Li, X.; Wang, C.; Pan, H.; Liu, W.; Wang, K.; Zeng, Q.; Wang, R.; Jiang, J. A Scalable General Synthetic Approach toward Ultrathin Imine-Linked Two-Dimensional Covalent Organic Framework Nanosheets for Photocatalytic CO_2 Reduction. *J. Am. Chem. Soc.* **2019**, *141*, 17431−17440.
(51) Garai, A.; Biradha, K. Cocrystals and Salts of 4,4′-Dinitro-2,2′,6,6′-tetracarboxybiphenyl with N-Heterocycles: Solid State Photodimerization of Criss-Cross Aligned Olefins and Photophysical Properties. *Cryst. Growth Des.* **2020**, *20*, 8059−8070.
(52) Moi, R.; Ghorai, A.; Banerjee, S.; Biradha, K. Amino- and Sulfonate-Functionalized Metal-Organic Framework for Fabrication of Proton Exchange Membranes with Improved Proton Conductivity. *Cryst. Growth Des.* **2020**, *20*, 5557−5563.
(53) Garai, M.; Biradha, K. Water-Resistant and Transparent Plastic Films from Functionalizable Organic Polymers:Coordination Polymers as Templates for Solid-State [2++2]-Photopolymerization. *Chem. - Eur. J.* **2017**, *23*, 273−277.
(54) Konavarapu, S. K.; Ghosh, D.; Dey, A.; Pradhan, D.; Biradha, K. Isostructural Ni^{II} Metal-Organic Frameworks (MOFs) for Efficient Electrocatalysis of Oxygen Evolution Reaction and for Gas Sorption Properties. *Chem. - Eur. J.* **2019**, *25*, 11141−11146.
(55) Mandal, R.; Garai, A.; Peli, S.; Datta, P. K.; Biradha, K. Photoinduced Bending of Single Crystals of a Linear Bis-Olefin via Water-Templated Solid-State [2 + 2] Photopolymerization Reaction. *Chem. - Eur. J.* **2020**, *26*, 396−400.
(56) Maity, K.; Nath, K.; Sinnwell, M. A.; Motkuri, R. K.; Thallapally, P. K.; Biradha, K. Isoreticular Expansion of Metal-Organic Frameworks via Pillaring of Metal Templated Tunable Building Layers: Hydrogen Storage and Selective CO_2 Capture. *Chem. - Eur. J.* **2019**, *25*, 14500−14505.
(57) Maity, K.; Karan, C. K.; Biradha, K. Porous Metal-Organic Polyhedral Framework containing Cuboctahedron Cages as SBUs with High Affinity for H_2 and CO_2 Sorption: A Heterogeneous Catalyst for Chemical Fixation of CO_2. *Chem. - Eur. J.* **2018**, *24*, 10988−10993.
(58) Howlader, P.; Zangrando, E.; Mukherjee, P. S. Self-Assembly of Enantiopure Pd12 Tetrahedral Homochiral Nanocages with Tetrazole Linkers and Chiral Recognition. *J. Am. Chem. Soc.* **2020**, *142*, 9070−9078.
(59) Mondal, B.; Mukherjee, P. S. Cage Encapsulated Gold Nanoparticles as Heterogeneous Photocatalyst for Facile and Selective Reduction of Nitroarenes to Azo Compounds. *J. Am. Chem. Soc.* **2018**, *140*, 12592−12601.
(60) Howlader, P.; Mondal, B.; Purba, P. C.; Zangrando, E.; Mukherjee, P. S. Self-Assembled Pd(II) Barrels as Containers for Transient Merocyanine Form and Reverse Thermochromism of Spiropyran. *J. Am. Chem. Soc.* **2018**, *140*, 7952−7960.
(61) Saha, R.; Devaraj, A.; Bhattacharyya, S.; Das, S.; Zangrando, E.; Mukherjee, P. S. Unusual Behavior of Donor-Acceptor Stenhouse Adducts in Confined Space of a Water-Soluble PdII8Molecular Vessel. *J. Am. Chem. Soc.* **2019**, *141*, 8638−8645.
(62) Prakasam, T.; Devaraj, A.; Saha, R.; Lusi, M.; Brandel, J.; Esteban-Gómez, D.; Platas-Iglesias, C.; Olson, M. A.; Mukherjee, P. S.; Trabolsi, A. Metal-Organic Self-Assembled Trefoil Knots for C—Br Bond Activation. *ACS Catal.* **2019**, *9*, 1907−1914.
(63) Bhattacharyya, S.; Venkateswarulu, M.; Sahoo, J.; Zangrando, E.; De, M.; Mukherjee, P. S. Self-Assembled Pt^{II}_8 Metallosupramolecular Tubular Cage as Dual Warhead Antibacterial Agent in Water. *Inorg. Chem.* **2020**, *59*, 12690−12699.
(64) Bhattacharyya, S.; Maity, M.; Chowdhury, A.; Saha, M. L.; Panja, S. K.; Stang, P. J.; Mukherjee, P. S. Coordination-Assisted Reversible Photoswitching of Spiropyran-Based Platinum Macrocycles. *Inorg. Chem.* **2020**, *59*, 2083−2091.
(65) Sinha, I.; Mukherjee, P. S. Chemical Transformations in Confined Space of Coordination Architectures. *Inorg. Chem.* **2018**, *57*, 4205−4221.
(66) Bhat, I. A.; Zangrando, E.; Mukherjee, P. S. Coordination-Driven Self-Assembly of Discrete Molecular Nanotubular Architectures. *Inorg. Chem.* **2019**, *58*, 11172−11179.
(67) Siddiqui, M. M.; Saha, R.; Mukherjee, P. S. Ruthenium(II) Metalla[2]catenanes and Macrocycles via Donor-Dependent Self-Assembly. *Inorg. Chem.* **2019**, *58*, 4491−4499.
(68) Das, P.; Kumar, A.; Chowdhury, A.; Mukherjee, P. S. Aggregation-Induced Emission and White Luminescence from a

Combination of π-Conjugated Donor-Acceptor Organic Luminogens. *ACS Omega* **2018**, *3*, 13757−13771.
(69) Bhattacharyya, S.; Chowdhury, A.; Saha, R.; Mukherjee, P. S. Multifunctional Self-Assembled Macrocycles with Enhanced Emission and Reversible Photochromic Behavior. *Inorg. Chem.* **2019**, *58*, 3968−3981.

https://dx.doi.org/10.1021/acs.inorgchem.1c00053
Inorg. Chem. 2021, 60, 5005−5013